IOP Publishing Journal of Physics A: Mathematical and Theoretical

J. Phys. A: Math. Theor. **50** (2017) 435302 (21pp) https://doi.org/10.1088/1751-8121/aa86cb

Spin-helix states in the *XXZ* spin chain with strong boundary dissipation

Vladislav Popkov[1,2], Johannes Schmidt[3] and Carlo Presilla[4,5]

[1] HISKP, University of Bonn, Nussallee 14-16, 53115 Bonn, Germany
[2] Centro Interdipartimentale per lo studio di Dinamiche Complesse, Università di Firenze, via G. Sansone 1, 50019 Sesto Fiorentino, Italy
[3] Institut für Teoretische Physik, Universität zu Köln, Zülpicher str. 77, Köln, Germany
[4] Dipartimento di Fisica, Sapienza Università di Roma, Piazzale Aldo Moro 2, Roma 00185, Italy
[5] Istituto Nazionale di Fisica Nucleare, Sezione di Roma 1, Roma 00185, Italy

E-mail: vladipopkov@gmail.com, schmidt@thp.uni-koeln.de and carlo.presilla@roma1.infn.it

Received 23 March 2017, revised 16 August 2017
Accepted for publication 17 August 2017
Published 27 September 2017

Abstract

We investigate the non-equilibrium steady state (NESS) in an open quantum XXZ chain attached at the ends to polarization baths with unequal polarizations. Using the general theory developed in Popkov (2017 *Phys. Rev.* A **95** 052131), we show that in the critical $XXZ\,|\Delta| < 1$ easy plane case, the steady current in large systems under strong driving shows resonance-like behaviour, by an infinitesimal change of the spin chain anisotropy or other parameters. Alternatively, by fine tuning the system parameters and varying the boundary dissipation strength, we observe a change of the NESS current from diffusive (of order $1/N$, for small dissipation strength) to ballistic regime (of order 1, for large dissipation strength). This drastic change results from an accompanying structural change of the NESS, which becomes a pure spin-helix state characterized by a winding number which is proportional to the system size. We calculate the critical dissipation strength needed to observe this surprising effect.

Keywords: non-equilibrium quantum systems, Lindblad equation, Heisenberg spin chain, boundary driven open quantum systems, steady state magnetization current

(Some figures may appear in colour only in the online journal)

The *XXZ* Heisenberg spin chain is a paradigmatic model in statistical mechanics. Its remarkable properties have long been known in the context of thermodynamic equilibrium [2, 3]. Recently, it was shown that the *XXZ* chain also retains many remarkable properties in a non-equilibrium setting, under a non-coherent boundary driving. An interesting strongly non-equilibrium instance of the problem occurs when a coherent evolution in the bulk is accompanied by a non-coherent local boundary driving, which tends to polarize the boundary spins along two different directions. If the boundary baths do not match, the system experiences a gradient of magnetization which leads to nonzero currents, even in the steady state. A schematic view of the model is shown in figure 1. Note that the alignment of the boundary spins to the respective baths cannot be made perfect, due to quantum fluctuations—except for the so-called Zeno limit, when the boundary dissipation is infinitely strong. An interplay between coherent bulk effects and incoherent boundary couplings results in the nontrivial scaling properties of the non-equilibrium steady state (NESS) characteristics (the currents, density profiles, many-point correlations, etc), which can be distinguished as different phases of criticality of the *XXZ* model [4–6].

The precise structure of the NESS for large systems and arbitrary mismatch of boundary polarizations is out of reach, because the complexity of the problem grows exponentially with the system size N. From the general setup of the problem, one would naively expect the NESS magnetization profile to interpolate between the left and right boundary, as depicted in figure 1. A few solvable cases, for which the NESS can be found analytically, [7] suggest that the system properties essentially depend on the phases of criticality of the *XXZ* model, characterized by the value of the spin exchange anisotropy Δ, while the NESS within each phase separately varies regularly and smoothly.

In the present communication we demonstrate that, contrary to expectations, the regular analytic behaviour of the NESS breaks down in a seemingly innocent and natural situation when the boundary driving is combined with an arbitrary spin-exchange anisotropy. We find that for a set of fine-tuned values of the anisotropy, various characteristics of the NESS, e.g. the magnetization current, may change dramatically, by orders of magnitude, and from monotonic behaviour to strongly non-monotonic, provided that the dissipative strength Γ becomes sufficiently large. For these special anisotropy values, and in their proximity as well, a structural transition in the NESS occurs, from a spatially smooth local magnetization profile interpolating between the boundary baths (small k in the Fourier space), to a rigid quasi-periodic structure of spins corresponding to large k values, arranged in a helix. Such a drastic structural transition naturally entails a singular behaviour of the NESS. Remarkably, the spin-helix state is a pure state, which is rather unusual for a many-body interacting quantum system dissipatively coupled to an external bath. Detuning the anisotropy or lowering the dissipation strength below a threshold value causes the spin-helix structure to relax back to a smooth profile. The set of critical anisotropies, at which the structural transitions to spin-helix state occur, becomes dense on the segment $[-1, 1]$ in the limit of large system size N.

The plan of the paper is as follows. We introduce the model and various properties of interest in section 1. In section 2 we review the conditions under which the pure NESS is achieved in the Zeno limit. In section 3 the convergence to an atypical NESS for finite dissipative strength is quantified, while in section 4 we characterize the points where this convergence fails. We discuss two possible experimental scenarios in section 5, and finally, in section 6, we draw our conclusions.

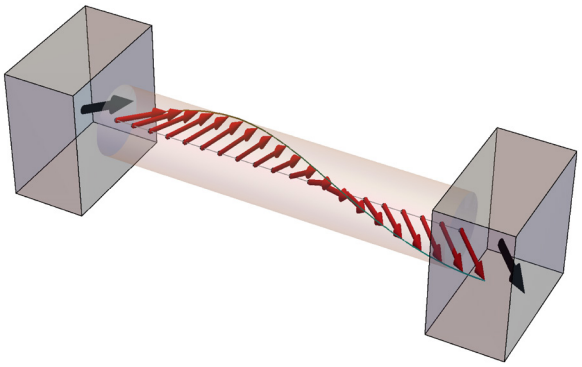

Figure 1. Schematic setup of a chain of spins attached to two fully polarizing boundary reservoirs. The chain has $N = 20$ spins and we have chosen boundary conditions $\theta_L = \theta_R = 0.4$, $\varphi_L = 0$, $\varphi_R = 4$.

1. Model

We consider an open *XXZ* chain coupled dissipatively to boundary reservoirs, described via the Lindblad master equation [8–10]

$$\frac{\partial \rho}{\partial t} = -\frac{\mathrm{i}}{\hbar}[H,\rho] + \sum_{\alpha} L_\alpha \rho L_\alpha^\dagger - \frac{1}{2}\left(L_\alpha^\dagger L_\alpha \rho + \rho L_\alpha^\dagger L_\alpha\right), \tag{1}$$

where H is the spin $1/2$ Heisenberg Hamiltonian with a partial anisotropy along the Z-axis

$$H_{XXZ} = \sum_{j=1}^{N-1} h_{jj+1}^{XXZ} = \sum_{j=1}^{N-1} J\left(\sigma_j^x\sigma_{j+1}^x + \sigma_j^y\sigma_{j+1}^y + \Delta\left(\sigma_j^z\sigma_{j+1}^z - I\right)\right). \tag{2}$$

The parameter Δ describes the Z-anisotropy. The Lindblad operators are chosen so as to target completely polarized states of the leftmost and rightmost spins (spins number 1 and number N, respectively). We parametrize the targeted boundary polarizations by polar and azimuthal angles θ_L, φ_L on the left end of the chain and θ_R, φ_R on its right end. We consider only two Lindblad operators, L_1, L_2, the first one being

$$L_1 = \frac{\sqrt{\Gamma}}{2}\left(-\sin\theta_L\sigma_1^z + (1+\cos\theta_L)\mathrm{e}^{-\mathrm{i}\varphi_L}\sigma_1^+ + (-1+\cos\theta_L)\mathrm{e}^{\mathrm{i}\varphi_L}\sigma_1^-\right), \tag{3}$$

where σ^α, $\alpha = x, y, z$, are Pauli matrices, lower indices denote the embeddings in the physical space, and $\sigma^\pm = (\sigma^x \pm \mathrm{i}\sigma^y)/2$. The second Lindblad operator, L_2, is obtained from equation (3) by the substitutions $\sigma_1^\alpha \to \sigma_N^\alpha$, $\theta_L \to \theta_R$, $\varphi_L \to \varphi_R$. It can be straightforwardly verified that the pure one-site state $\rho_L = |\psi_1\rangle\langle\psi_1|$, with $\langle\psi_1| = \langle\cos(\theta_L/2)\mathrm{e}^{-\mathrm{i}\varphi_L/2}, \sin(\theta_L/2)\mathrm{e}^{\mathrm{i}\varphi_L/2}|$, is a dark state of L_1, i.e. $L_1|\psi_1\rangle = 0$. In the absence of the coherent evolution term in equation (1), the left boundary spin relaxes to a state $\rho_L = |\psi_1\rangle\langle\psi_1| = \frac{1}{2}\vec{l}_L\vec{\sigma}_1$, with $\vec{l}_L = (\sin\theta_L\cos\varphi_L, \sin\theta_L\sin\varphi_L, \cos\theta_L)$, with a characteristic time $\tau = \Gamma^{-1}$. An analogous statement holds for the rightmost spin, which (in the absence of the coherent evolution) becomes polarized along the direction $\vec{l}_R = (\sin\theta_R\cos\varphi_R, \sin\theta_R\sin\varphi_R, \cos\theta_R)$. A possible experimental protocol of repeating interactions leading to the density matrix evolution (1) and (3) is discussed in [11]. It is clear that any non-fully-matching boundary conditions, $(\theta_L, \varphi_L) \neq (\theta_R, \varphi_R)$, introduce a boundary mismatch, and result in steady currents

flowing through the chain. In particular, due to the spin-exchange anisotropy in XY-plane, the Z-component of the magnetization current j^z is locally conserved.

In the following solvable cases, the NESS—specifically, the time-independent solution of equation (1), is known analytically:

Collinear boundary driving along the anisotropy axis $\varphi_L = \varphi_R = 0, \theta_L = 0, \theta_R = \pi$ [6]. The steady magnetization current is ballistic in the critical regime $|\Delta| < 1$, is exponentially small in the Ising-like case $|\Delta| > 1$, and is subdiffusive in the isotropic case $\Delta = 1$. For large Γ, the Z-component of the magnetization current j^z vanishes due to the quantum Zeno effect.

Non-collinear XY-plane boundary driving $\varphi_L = 0, \varphi_R = \Phi, \theta_L = \theta_R = \pi/2$ *and isotropic Heisenberg model* $\Delta = 1$ [12, 13]. In the isotropic case, all components of the magnetization current are conserved. The components j^x, j^y are subdiffusive, and decrease for large Γ, due to the quantum Zeno effect, while j^z increases monotonically with Γ. The NESS-dependence on Γ is regular and piecewise monotonic.

Non-collinear strong XY-plane boundary driving and fine-tuned anisotropy Δ. It was suggested in [14], that for sufficiently strong dissipative coupling, the NESS becomes arbitrarily close to a pure state, which we shall call the spin-helix state (SHS), in analogy to states appearing in two-dimensional electron systems with spin–orbit coupling [15–17], $\lim_{\Gamma\to\infty} \rho_{\rm NESS}(\Gamma) = |\Psi_{\rm SHS}\rangle \langle\Psi_{\rm SHS}|$, where

$$|\Psi_{\rm SHS}\rangle = 2^{-\frac{N}{2}} \bigotimes_{k=1}^{N} \begin{pmatrix} {\rm e}^{-\frac{\rm i}{2}\varphi(k-1)} \\ {\rm e}^{\frac{\rm i}{2}\varphi(k-1)} \end{pmatrix}, \tag{4}$$

provided the states of the boundary spins match the boundary driving, viz. $\theta_L = \theta_R = \pi/2$, $\varphi_L = 0, \varphi_R \equiv (N-1)\varphi = \Phi$, and the anisotropy Δ obeys

$$\Delta = \cos\varphi. \tag{5}$$

In the present situation, when the Lindblad operators (3) are targeting pure single-spin states, the SHSs (4) are obtained in an ideal Zeno regime $\Gamma \to \infty$. Note, however, that it is also possible to generate the same SHSs for finite dissipative strengths Γ, if fine-tuned mixed single-spin states at the boundaries are dissipatively targeted [18].

The SHSs (4) are quite remarkable in many respects. From the point of view of a dissipative dynamics, the creation of a pure quantum state via a dissipative action is a way to beat detrimental decoherence effects. From the point of view of spintronics, the state (4) carries an anomalously high ballistic magnetization current of order 1, which is independent of the system size.

The existence of SHS in the Zeno limit at fine-tuned anisotropy (5) was guessed in [14] on the basis of a necessary criterion and explicit calculation of the NESS for small system sizes. Here we revisit and systematically treat the SHS on the basis of a general theory (which provides necessary and sufficient criteria for SHS existence, and also a convergence criterion) developed by us in [1]. We treat a more general SHS,

$$|\Psi_{\rm SHS}\rangle = \bigotimes_{k=1}^{N} \begin{pmatrix} \cos(\frac{\theta}{2}){\rm e}^{-\frac{\rm i}{2}\varphi(k-1)} \\ \sin(\frac{\theta}{2}){\rm e}^{\frac{\rm i}{2}\varphi(k-1)} \end{pmatrix}, \tag{6}$$

which, as we shall see later, can be dissipatively generated in a boundary driven XXZ spin chain by tuning the boundary conditions and the anisotropy. The state (6) describes a precession, along the chain, of the local spin around the Z-axis, forming a frozen spin wave structure—see figure 1 for an illustration—with constant twisting azimuthal angle difference φ between two neighbouring spins. This is evident if we compute the expectation value of the local spin at site n

$$\langle\Psi_{\rm SHS}|\,\vec{\sigma}_n\,|\Psi_{\rm SHS}\rangle = (\sin\theta\cos\varphi(n-1), \sin\theta\sin\varphi(n-1), \cos\theta). \tag{7}$$

The local spin orientations obtained in a chain with $N = 20$ spins and boundary conditions $\theta_L = \theta_R = 0.4$, $\varphi_L = 0$, $\varphi_R = 4$ are shown in figure 1.

Note that fixed boundary polarizations $\varphi_L = 0, \varphi_R = \Phi$ match not just one SHS (6) with $\varphi(N-1) = \Phi$, but also those with $\varphi(N-1) = \Phi + 2\pi$, $\varphi(N-1) = \Phi + 4\pi$ etc, until $\varphi(N-1) = \Phi + (N-2)2\pi$. Thus, we shall also characterize an SHS via a winding number $m = \lfloor (N-1)\varphi/(2\pi) \rfloor$, $\lfloor \cdot \rfloor$ being the integer part.

We will see in the following that the SHSs (6) constitute the points of resonance-like behaviour of the NESS, which becomes visible at large dissipation. In doing so, we shall answer some basic questions. How large must the dissipation strength be to reach the limiting SHS with a predefined accuracy? To what extent are the characteristics of the SHS/states *atypical* for given boundary mismatch? Can the resonance-like behaviour be detected in other features of the NESS? What happens if the system gets larger and larger, and, eventually, we reach the thermodynamic limit of infinitely long chains?

The characterization of several properties of the NESS prove to be useful for our later considerations.

(a) A measure of the purity. In fact, in driven Heisenberg spin chains with polarization targeting operators, a NESS can become pure, e.g. $\rho_{\rm NESS} = |\Psi_{\rm SHS}\rangle \langle \Psi_{\rm SHS}|$, where $|\Psi_{\rm SHS}\rangle$ is the SHS (6), *only* in the Zeno limit. As a criterion for purity of a state ρ, we shall use both the von Neumann entropy, $S_{\rm VNE}(\rho) = -\,{\rm tr}(\rho \log_2 \rho)$, and the alternative measure $\epsilon(\rho) = 1 - {\rm tr}(\rho^2)$.

(b) Steady currents of magnetization and of energy. Being a non-equilibrium steady state, the NESS is characterized by non-vanishing steady currents. The magnetization (spin) current operator in the Z-direction, $\hat{\jmath}_{n,n+1}$, is defined via a lattice continuity equation $\frac{\rm d}{{\rm d}t}\sigma_n^z = \hat{\jmath}_{n-1,n} - \hat{\jmath}_{n,n+1}$, where

$$\hat{\jmath}_{n,m} = J(\sigma_n^x \sigma_m^y - \sigma_n^y \sigma_m^x). \tag{8}$$

The energy current operator, $\hat{J}_n^E$, is defined analogously by $\frac{\rm d}{{\rm d}t} h_{n,n+1} = \hat{J}_n^E - \hat{J}_{n+1}^E$, where

$$\hat{J}_n^E = -\sigma_n^z \hat{\jmath}_{n-1,n+1} + \Delta(\hat{\jmath}_{n-1,n}\sigma_{n+1}^z + \sigma_{n-1}^z \hat{\jmath}_{n,n+1}). \tag{9}$$

(c) Finally, we need a cumulative function characterizing the density profile σ_n^α, which probes the helix structure of the spins. To this end, we introduce a generalized structure factor (or, alternatively, a generalized discrete Fourier transform (GFT)), via

$$\hat{f}_m(\Phi) = \frac{1}{M}\sum_{k=0}^{M-1} f_k {\rm e}^{-{\rm i}\varphi(m)k}, \tag{10}$$

where

$$\varphi(m) = \frac{\Phi + 2\pi m}{M}, \qquad m = 0, 1, \ldots, M-1. \tag{11}$$

Here, $M + 1 = N$ is the chain length, $0 \leqslant \Phi < 2\pi$ and m is the winding number. For $\Phi = 0$, equation (10) turns into the usual discrete Fourier transform. The GFT shares similar properties with the usual Fourier transform, e.g. the Parseval identity has the usual form

$$\sum_{m=0}^{M-1} |\hat{f}_m(\Phi)|^2 = \frac{1}{M}\sum_{k=0}^{M-1} |f_k|^2. \tag{12}$$

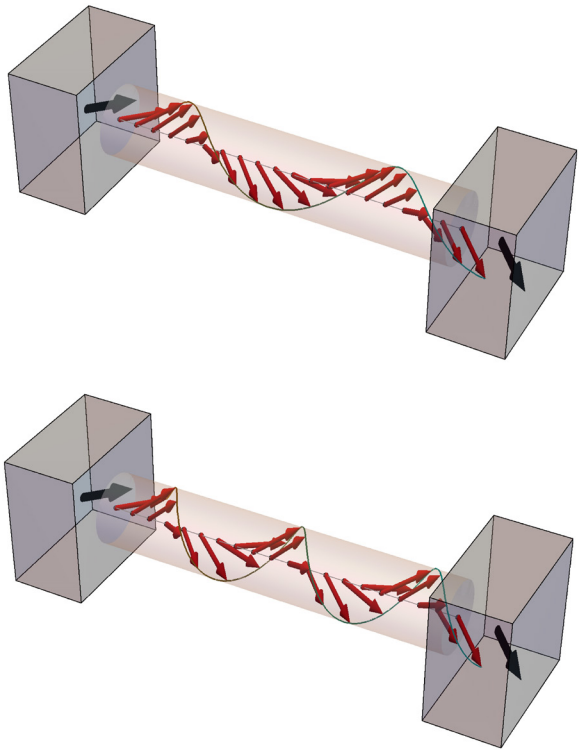

Figure 2. SHSs as in figure 1 but with winding numbers $m = 1$ (top) and $m = 2$ (bottom).

A convenient quantity to look at is the GFT (10) of the one-point observables

$$f_{k-1} = \mathrm{tr}((\sigma_k^x + i\sigma_k^y)\rho), \qquad k = 1, 2, \ldots, N-1, \tag{13}$$

which play the role of the usual Fourier harmonics. Indeed, for a SHS with winding number m_0, we find $f_k = \mathrm{e}^{\mathrm{i}\varphi(m_0)k}$.

The above quantities (a)–(c) are easily calculated for the stationary SHS $\rho_{\mathrm{SHS}} = |\Psi_{\mathrm{SHS}}\rangle\langle\Psi_{\mathrm{SHS}}|$, where $|\Psi_{\mathrm{SHS}}\rangle$ is given by equation (6) with $\varphi = \varphi(m_0) = (\Phi + 2\pi m_0)/(N-1)$, yielding

$$S_{\mathrm{VNE}}(\rho_{\mathrm{SHS}}) = \epsilon(\rho_{\mathrm{SHS}}) = 0, \tag{14}$$

$$j^z(\rho_{\mathrm{SHS}}) = \mathrm{tr}(\hat{\jmath}_{n,n+1}\rho_{\mathrm{SHS}}) = J\sin\theta\sin\varphi(m_0), \tag{15}$$

$$J_E(\rho_{\mathrm{SHS}}) = \mathrm{tr}(\hat{J}_n^E\rho_{\mathrm{SHS}}) = 0, \tag{16}$$

$$\hat{f}_m(\Phi) = \sin\theta\delta_{m,m_0}, \qquad m = 0, 1, \ldots, N-2. \tag{17}$$

We stress that the SHS is realized as a NESS of the system only in the ideal limit $\Gamma \to \infty$. To see how the above quantities change in the physically more relevant situation of finite Γ, consider first a simple yet demonstrative example. Figures 3 and 4 show the von Neumann entropy of the actual ρ_{NESS} and the corresponding steady-state magnetization current j^z as a function of the anisotropy Δ for fixed N, θ and Φ, for two—large and small—values of the

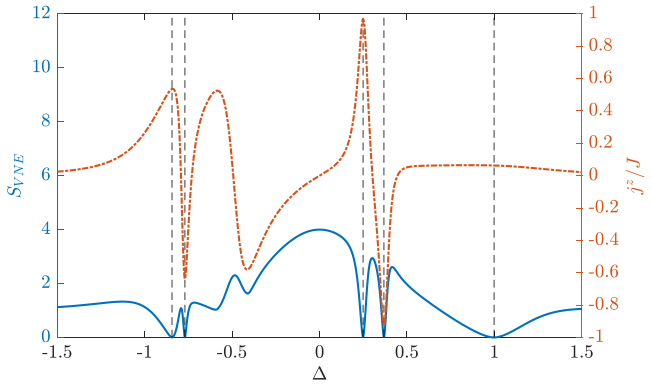

Figure 3. von Neumann entropy (solid blue line,left vertical scale) of the NESS and steady-state magnetization current (dot-dashed red line, right vertical scale) versus the anisotropy Δ for $\Gamma = 1000$. The minima of $S_{\rm VNE}$ correspond to almost pure SHSs with different winding numbers. The vertical dashed lines indicate the critical anisotropies of equation (18) obtained, from left to right, for $m = 2, 3, 4, 1, 0$. System parameters: $N = 6$, $\theta = \pi/2$, $\Phi = \pi/10$.

dissipation strength Γ (for a quantification of the notions 'large' and 'small' see section 3). The NESS is found by solving equation (1) numerically.

For large Γ, in figure 3 we see that for values of the anisotropy Δ given by

$$\Delta_{\rm cr}(m, \Phi) = \cos \frac{\Phi + 2\pi m}{N - 1}, \qquad m = 0, 1, \ldots, N - 2, \tag{18}$$

$\rho_{\rm NESS}$ becomes a pure state—specifically, an SHS with winding number m. For the same value of Γ, the steady-state magnetization current abruptly changes sign and amplitude in the region $\Delta \in [-1, 1]$ depending on the value of $\sin \varphi(m)$. For small Γ—see figure 4—the above pure-state features fade away for both $S_{\rm VNE}$ and j^z.

If the polarizations of the boundary spins of the chain differ slightly, as in the example shown in figures 3 and 4, where the boundary angle mismatch is $\Phi = \pi/10$, one would expect a steady magnetization current proportional to the bulk gradient $\Phi/(N - 1)$. In fact, naively, one may assume that neighbouring spins $k, k + 1$ are almost collinear in the steady state. This scenario indeed happens for small Γ, and, if Γ is large, for Δ away from the critical values (18), where the spins arrange in a helical structure with angle between neighbouring spins $\varphi = (\Phi + 2\pi m)/(N - 1)$, $m = 0, 1, \ldots, N - 2$. On the other hand, at the critical values of Δ corresponding to winding numbers $m > 0$, a resonance takes place, with a drastic increase of the amplitude of the steady current j^z. As the system size grows, the magnetization current and the von Neumann entropy peaks become narrower and steeper.

To verify the existence of the helical arrangement of the spins in the regions near the critical values of the anisotropy, it is instructive to look at the GFT coefficients $\hat{f}_m$ of equation (10) as a function of the anisotropy. As shown in figures 5 and 6, the GFT coefficients $\hat{f}_m$ reach their absolute maxima exactly at the points $\Delta_{\rm cr}(m, \Phi)$, in agreement with the prediction of equation (17). This allows us to conclude that the pure states evidenced in figure 4 by the vanishing of $S_{\rm VNE}$ are, in fact, the SHSs (6). Note that, for large Γ, i.e. in figure 5, the amplitudes of the maxima of the coefficients $\hat{f}_m$ are independent of m, and coincide with the value $\sin\theta$ predicted by equation (17).

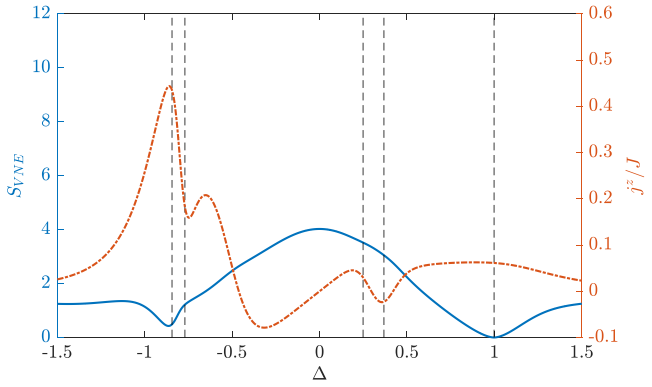

Figure 4. As in figure 3 for $\Gamma = 10$.

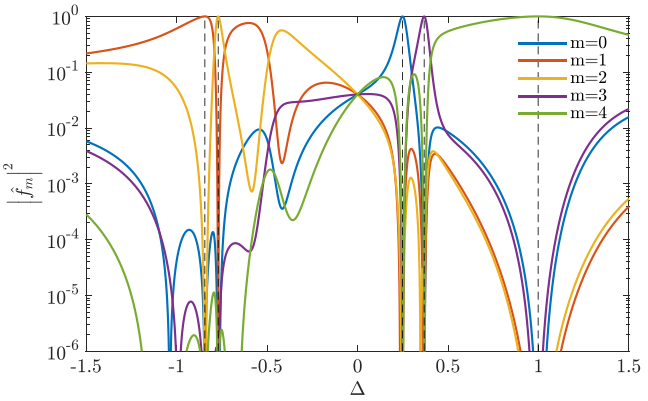

Figure 5. Generalized Fourier coefficients $\hat{f}_m$ versus the anisotropy Δ for $\Gamma = 1000$. System parameters as in figure 3.

2. Boundary driven *XXZ* spin chain: criterion for NESS purity

In order for the NESS to be pure in the Zeno limit, we require an existence of a NESS expansion in powers of $1/\Gamma$,

$$\rho_{\rm NESS}(\Gamma) = \sum_{m=0}^{\infty} \frac{\rho^{(m)}}{\Gamma^m}, \tag{19}$$

where the zeroth order term is a pure state,

$$\rho^{(0)} = |\Psi\rangle\langle\Psi|. \tag{20}$$

Consistency of the expansion (19) with the purity assumption (20) leads to restrictions for the effective Hamiltonian H. The general theory [1] predicts that, for boundary driven systems, in the Zeno limit a pure steady state $\rho_{\rm NESS} = |\Psi\rangle\langle\Psi|$ can be targeted, where $|\Psi\rangle = |\psi_{\rm Zeno}\rangle \otimes |\psi_{\rm target}\rangle$, with $|\psi_{\rm Zeno}\rangle \in \mathcal{H}_0$ and $|\psi_{\rm target}\rangle \in \mathcal{H}_1$, $\mathcal{H}_0$ being the Hilbert subspace where the dissipation (Lindblad operators) acts and $\mathcal{H}_1$ its complement with respect

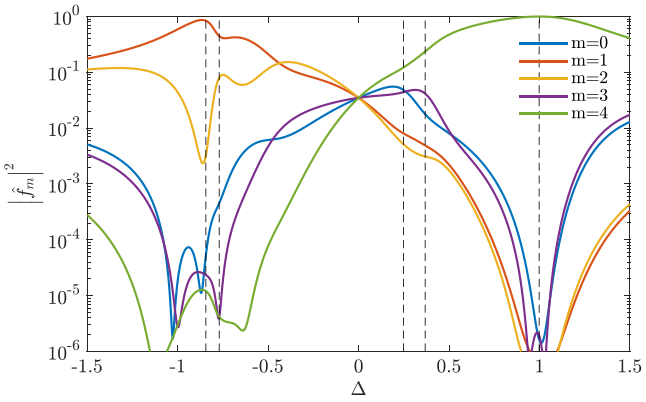

Figure 6. As in figure 5 for $\Gamma = 10$.

to the whole Hilbert space, $\mathcal{H} = \mathcal{H}_0 \otimes \mathcal{H}_1$. A necessary condition for this NESS purity to be achieved is that

$$H|\Psi\rangle = \lambda|\Psi\rangle + \kappa \left|\psi^{\perp}_{\text{Zeno}}\right\rangle \otimes |\psi_{\text{target}}\rangle, \tag{21}$$

where $\left|\psi^{\perp}_{\text{Zeno}}\right\rangle \in \mathcal{H}_0$ is a state orthogonal to $|\psi_{\text{Zeno}}\rangle$, $\kappa \neq 0$, and λ is an arbitrary real constant. The criterion (21) gives a necessary condition, while two extra conditions must be checked to guarantee the convergence of the NESS to the targeted pure state $|\Psi\rangle$ in the Zeno limit. These extra conditions will be discussed in section 4.

The validity of the purity criterion (21) for the Heisenberg Hamiltonian with the boundary spins 1 and N attached to polarizing reservoirs stems from the following property of the local Hamiltonian density $h^{XXZ}_{j,j+1}(\Delta)$, with $\Delta = \cos\varphi$,

$$h^{XXZ}_{j,j+1}(\cos\varphi)\,|\psi(\theta,\alpha)\rangle_j \otimes |\psi(\theta,\alpha+\varphi)\rangle_{j+1} = -\mathrm{i}J\sin\theta\sin\varphi \times \left(\left|\psi^{\perp}(\theta,\alpha)\right\rangle_j \otimes |\psi(\theta,\alpha+\varphi)\rangle_{j+1} - |\psi(\theta,\alpha)\rangle_j \otimes \left|\psi^{\perp}(\theta,\alpha+\varphi)\right\rangle_{j+1}\right), \tag{22}$$

where the lower index in a state denotes the respective embedding and

$$|\psi(\theta,\alpha)\rangle = \begin{pmatrix} \cos\frac{\theta}{2}\mathrm{e}^{-\mathrm{i}\alpha/2} \\ \sin\frac{\theta}{2}\mathrm{e}^{\mathrm{i}\alpha/2}, \end{pmatrix} \tag{23}$$

$$\left|\psi^{\perp}(\theta,\alpha)\right\rangle = \begin{pmatrix} \sin\frac{\theta}{2}\mathrm{e}^{-\mathrm{i}\alpha/2} \\ -\cos\frac{\theta}{2}\mathrm{e}^{\mathrm{i}\alpha/2} \end{pmatrix}. \tag{24}$$

It is simple to verify that equation (21) is satisfied with $\lambda = 0, \kappa = -\mathrm{i}J\sqrt{2}\sin\theta\sin\varphi$, and

$$|\psi\rangle_{\text{Zeno}} = |\psi(\theta,0)\rangle_1 \otimes |\psi(\theta,\Phi)\rangle_N, \tag{25}$$

$$|\psi\rangle^{\perp}_{\text{Zeno}} = \frac{1}{\sqrt{2}}\left(\left|\psi^{\perp}(\theta,0)\right\rangle_1 \otimes |\psi(\theta,\Phi)\rangle_N - |\psi(\theta,0)\rangle_1 \otimes \left|\psi^{\perp}(\theta,\Phi)\right\rangle_N\right), \tag{26}$$

$$|\psi_{\text{target}}\rangle = \bigotimes_{j=2}^{N-1} |\psi(\theta,(j-1)\varphi)\rangle_j. \tag{27}$$

Note that in the above three states we have $\alpha = 0$ and $\varphi = (\Phi + 2\pi m)/(N-1)$, with m integer. We conclude that the stationary pure state approached in the Zeno limit (fully polarizing reservoirs), viz.

$$|\Psi\rangle = \bigotimes_{j=1}^{N} |\psi(\theta, (j-1)\varphi)\rangle_j , \tag{28}$$

is the SHS anticipated in equation (6). It describes a 'homogeneous' spin precession around the anisotropy axis Z along the chain, with a constant polar angle θ and a monotonically increasing azimuthal angle $(j-1)\varphi$, $j = 1, 2, \ldots, N$, matching the boundary values $(\sin\theta, 0, \cos\theta)$ and $(\sin\theta\cos\Phi, \sin\theta\sin\Phi, \cos\theta)$. Indeed, the expectation value of the spin projection at site j is

$$\begin{aligned}\langle \vec{\sigma}_j \rangle &= \mathrm{tr}\left(|\psi(\theta,(j-1)\varphi)\rangle \langle \psi(\theta,(j-1)\varphi)| \vec{\sigma}\right) \\ &= (\sin\theta\cos(j-1)\varphi, \sin\theta\sin(j-1)\varphi, \cos\theta).\end{aligned} \tag{29}$$

For $\theta = \pi/2$, we have the simpler helix-state of equation (4), describing spins which locally rotate entirely in the XY plane.

Whereas the criterion (21) ensures that the NESS converges to the spin-helix pure state in the limit $\Gamma \to \infty$, the general theory developed in [1] allows us to quantify the speed of this convergence by establishing a characteristic dissipation, as discussed in the next section.

3. Convergence to the SHS for finite dissipation strength

According to [1], we introduce an orthonormal basis $|e^j\rangle$ in the subspace $\mathcal{H}_0$ where dissipation acts and split the Hamiltonian H with respect to this basis. In our present case $\mathcal{H}_0$ is the direct product of the local spin spaces corresponding to the sites 1 and N,

$$H = \sum_{j=0}^{d_0-1}\sum_{k=0}^{d_0-1} H_{jk} = \sum_{j=0}^{d_0-1}\sum_{k=0}^{d_0-1} |e^j\rangle\langle e^k| \otimes h^{jk}, \tag{30}$$

where $d_0 = 4$ is the dimension of $\mathcal{H}_0$. The first two basis vectors are chosen as $|e^0\rangle \equiv |\psi_{\mathrm{Zeno}}\rangle$ and $|e^1\rangle \equiv |\psi^{\perp}_{\mathrm{Zeno}}\rangle$, with $|\psi_{\mathrm{Zeno}}\rangle$ and $|\psi^{\perp}_{\mathrm{Zeno}}\rangle$ defined as in equations (25) and (26) respectively. The other vectors of the basis are chosen as (subscript indices denote the embedding)

$$|e^2\rangle = \frac{1}{\sqrt{2}}\left(|\psi^{\perp}(\theta,0)\rangle_1 |\psi(\theta,\Phi)\rangle_N + |\psi(\theta,0)\rangle_1 |\psi^{\perp}(\theta,\Phi)\rangle_N\right), \tag{31}$$

$$|e^3\rangle = |\psi^{\perp}(\theta,0)\rangle_1 |\psi^{\perp}(\theta,\Phi)\rangle_N . \tag{32}$$

Having defined the basis in the $\mathcal{H}_0$, the coefficients h^{jk} of the decomposition (30), which are operators in $\mathcal{H}_1$, are readily calculated as

$$h^{jk} = \mathrm{tr}_{1,N}\left(\left(|e^k\rangle\langle e^j| I_{2,3,\ldots,N-1}\right) H\right), \tag{33}$$

where $I_{2,3,\ldots,N-1}$ is the identity operator in the space of spins $2, 3, \ldots, N-1$, and

$$\mathrm{tr}_{1,N}(\cdot) = \mathrm{tr}_N(\mathrm{tr}_1(\cdot)), \tag{34}$$

$$\mathrm{tr}_n(\cdot) = (\langle +|\cdot|+\rangle)_n + (\langle -|\cdot|-\rangle)_n , \qquad n = 1, 2, \ldots, N, \tag{35}$$

where $|\pm\rangle$ are the eigenstates of σ^z.

Of special importance is the term h^{00}, which is the projection of the Hamiltonian H on the state $\left|e^0\right\rangle$ targeted by the dissipation. In fact, we have $\mathcal{D}_1\left|e^0\right\rangle\left\langle e^0\right| = \mathcal{D}_N\left|e^0\right\rangle\left\langle e^0\right| = 0$, where $\mathcal{D}_1$ and $\mathcal{D}_N$ are the dissipators associated to the Lindblad operators L_1 and L_N, e.g. $\mathcal{D}_1\rho = L_1\rho L_1^\dagger - \frac{1}{2}(L_1^\dagger L_1\rho + \rho L_1^\dagger L_1)$. From equation (33) and after some algebra, we obtain

$$h^{00} = H' + C_{++}(2,\theta,0) + C_{++}(N-1,\theta,\Phi), \tag{36}$$

$$H' = \sum_{j=2}^{N-2} h^{XXZ}_{j,j+1}(\Delta), \tag{37}$$

$$\begin{aligned} C_{++}(m,\theta,\varphi) &= \mathrm{tr}_{m-1}\left(\left(|\psi(\varphi)\rangle\langle\psi(\varphi)|\right)_{m-1} h^{XXZ}_{m-1,m}\right) \\ &= J(\sin\theta(\mathrm{e}^{\mathrm{i}\varphi}\sigma_m^- + \mathrm{e}^{-\mathrm{i}\varphi}\sigma_m^+) + \Delta\sigma_m^z\cos\theta - \Delta I_{2,3,\ldots,N-1}), \end{aligned} \tag{38}$$

where $h^{XXZ}_{j,j+1}$ are the local energy densities of the *XXZ* Hamiltonian (2) and $\sigma_m^\alpha = I_{2,3,\ldots,m-1}\otimes\sigma^\alpha\otimes I_{m+1,\ldots,N-1}$, with $1\leqslant m\leqslant N$ and $\alpha = \pm, z$. Provided equation (21) is satisfied, the target state is an eigenstate of h^{00} with eigenvalue λ,

$$h^{00}\left|\psi_{\text{target}}\right\rangle = \lambda\left|\psi_{\text{target}}\right\rangle. \tag{39}$$

Defining also

$$\begin{aligned} C_{-+}(m,\theta,\varphi) &= \mathrm{tr}_{m-1}\left(\left(\left|\psi^\perp(\varphi)\right\rangle\langle\psi(\varphi)|\right)_{m-1} h^{XXZ}_{m-1,m}\right) \\ &= J\left(2\sin^2\frac{\theta}{2}\left(\mathrm{e}^{-\mathrm{i}\varphi}\sigma_m^+\right) - 2\cos^2\frac{\theta}{2}\left(\mathrm{e}^{\mathrm{i}\varphi}\sigma_m^-\right) + \Delta\sigma_m^z\sin\theta\right), \end{aligned} \tag{40}$$

$$\begin{aligned} C_{+-}(m,\theta,\varphi) &= \mathrm{tr}_{m-1}\left(\left(|\psi(\varphi)\rangle\left\langle\psi^\perp(\varphi)\right|\right)_{m-1} h^{XXZ}_{m-1,m}\right) \\ &= (C_{-+}(m,\theta,\varphi))^\dagger, \end{aligned} \tag{41}$$

$$\begin{aligned} C_{--}(m,\theta,\varphi) &= \mathrm{tr}_{m-1}\left(\left(\left|\psi^\perp(\varphi)\right\rangle\left\langle\psi^\perp(\varphi)\right|\right)_{m-1} h^{XXZ}_{m-1,m}\right) \\ &= J\left(-\sin\theta\left(\mathrm{e}^{\mathrm{i}\varphi}\sigma_m^- + \mathrm{e}^{-\mathrm{i}\varphi}\sigma_m^+\right) - \Delta\cos\theta\sigma_m^z - \Delta I_{2,3,\ldots,N-1}\right), \end{aligned} \tag{42}$$

and denoting $\varphi_L = 0$ and $\varphi_R = \Phi$, we obtain the following other components h^{jk}:

$$h^{01} = \frac{1}{\sqrt{2}}\left(C_{-+}(2,\theta,\varphi_L) - C_{-+}(N-1,\theta,\varphi_R)\right), \tag{43}$$

$$h^{02} = \frac{1}{\sqrt{2}}\left(C_{-+}(2,\theta,\varphi_L) + C_{-+}(N-1,\theta,\varphi_R)\right), \tag{44}$$

$$h^{03} = 0, \qquad \text{for} N > 2, \tag{45}$$

$$\begin{aligned} h^{21} = \frac{1}{2}\big(&C_{++}(N-1,\theta,\varphi_R) - C_{--}(N-1,\theta,\varphi_R) \\ &+ C_{--}(2,\theta,\varphi_L) - C_{++}(2,\theta,\varphi_L)\big), \end{aligned} \tag{46}$$

$$h^{31} = \frac{1}{\sqrt{2}}\left(-C_{+-}(2,\theta,\varphi_L) + C_{+-}(N-1,\theta,\varphi_R)\right), \tag{47}$$

$$h^{11} = H' - 2\Delta I_{2,3,\ldots,N-1}, \tag{48}$$

$$h^{jk} = (h^{kj})^{\dagger}. \tag{49}$$

The remaining h^{jk} are obtained analogously.

On using equations (36) and (43)–(47), we can compute the characteristic value of the dissipation Γ, beyond which the NESS differs from the pure SHS (28) for less than a chosen error. In fact, according to [1], if the criterion (21) is satisfied, then, not only $\lim_{\Gamma\to\infty}\rho_{\rm NESS}(\Gamma) = |\Psi\rangle\langle\Psi|$, where $|\Psi\rangle$ is given by equation (28), but for finite Γ we have that the NESS is characterized by a purity index

$$\epsilon(\Gamma) = 1 - \mathrm{tr}\,\rho_{\rm NESS}(\Gamma)^2 = \frac{\Gamma_{\rm ch}^2}{\Gamma^2} + o\left(\frac{1}{\Gamma^2}\right), \tag{50}$$

whose value is determined by the squared ratio between Γ and a characteristic dissipation. The latter is given by the formula

$$(\Gamma_{\rm ch})^2 = 8|\kappa|^2 \sum_{\alpha=1}^{d_1-1}\sum_{\beta=1}^{d_1-1}(K^{-1})_{\alpha\beta}R_\beta, \tag{51}$$

where K is the $(d_1-1)\times(d_1-1)$, $d_1 = 2^{N-2}$, matrix having elements

$$K_{\alpha\beta} = \sum_{k=1}^{d_0-1}\left(\left|\langle\alpha|h^{k0}|\beta\rangle\right|^2 - \delta_{\alpha\beta}\langle\alpha|(h^{k0})^{\dagger}h^{k0}|\alpha\rangle\right), \qquad \alpha,\beta = 1,2,\ldots,d_1-1, \tag{52}$$

and

$$R_\alpha = \langle\alpha|F|\psi_{\rm target}\rangle\langle\psi_{\rm target}|F^{\dagger}|\alpha\rangle, \qquad \alpha = 1,2,\ldots,d_1-1, \tag{53}$$

with

$$F = \sum_{k=1}^{d_0-1}\left(h^{k1} + \left[\Lambda h^{01}, h^{k0}\right]\right), \tag{54}$$

and

$$\Lambda = \sum_{\alpha=1}^{d_1-1}\frac{1}{\lambda_\alpha - \lambda}|\alpha\rangle\langle\alpha|. \tag{55}$$

The symbols λ_α indicate the eigenvalues of h^{00} for $\alpha = 1,\ldots,d_1-1$, whereas $\lambda \equiv \lambda_0$, also entering the condition (21), is the principal eigenvalue of h^{00}—see equation (39).

In agreement with the results of the previous section, for $\Delta = \cos\varphi$ and $\varphi = (\Phi + 2\pi p)/(N-1)$, with p integer, we find

$$\lambda = 0, \tag{56}$$

which follows from the easily checkable identity

$$C_{++}(m,\theta,\Phi)\,|\psi(\theta,\Phi+\varphi)\rangle = (\cos\varphi-\Delta)\,|\psi(\theta,\Phi+\varphi)\rangle + \left(\mathrm{i}\sin\varphi\sin\theta-\frac{1}{2}\sin 2\theta\,(\cos\varphi-\Delta)\right)|\psi^{\perp}(\theta,\Phi+\varphi)\rangle \tag{57}$$

and equations (39) and (36).

4. Divergences of the characteristic dissipation

If Λ and K^{-1} are nonsingular matrices, the characteristic value of the dissipation $\Gamma_{\rm ch}$ is always finite, and the NESS converges to the SHS (6) for $\Gamma \gg \Gamma_{\rm ch}$. On the other hand, divergence of $\Gamma_{\rm ch}$ signifies a breakdown of the purity assumption (20), and consequently the breakdown of the convergence to the SHS in the Zeno limit.

Points of divergence of $\Gamma_{\rm ch}$ may happen when Λ or K^{-1} is singular. In our problem, we have three parameters: the twisting angle φ, the polar angle θ, and the size of the system N—the anisotropy being fixed by equation (21) to be $\Delta=\cos\varphi$. Investigating, with the help of Mathematica, the analytic expression (51) for $N\leqslant 12$ leads us to formulate the following ansatz.

Ansatz. For any finite size $N\geqslant 3$ and any fixed $0<\theta<\pi$, $\Gamma_{\rm ch}(\varphi)$ diverges at a set of isolated singular points $\varphi_j^*\in\Omega_N$, given by

$$\Omega_N=\left\{\varphi_j^*:\ \varphi_j^* k=\pi d,\ k=2,3,\ldots,N-1,\ d\in\mathbb{Z}\right\}. \tag{58}$$

Moreover, in the ϵ-vicinity of every point φ_j^*, we have $\Gamma_{\rm ch}(\varphi_j^*+\epsilon)=A_0(N,\theta,\varphi_j^*)|\epsilon|^{-a_j}$, with $a_j=1$.

4.1. Effective number of $\Gamma_{\rm ch}$ singularities

The condition (58) has a very simple geometrical interpretation: it marks all possible twisting angles φ for which the target SHS has two or more collinear spins including the boundary spins. It is enough to describe the points of Ω_N lying in the segment $]0,\pi[$. In fact, inverting the sign of a φ_j^* changes the sign of the helicity but conserves the collinearity of the spins. We also exclude the trivial points $\varphi_j^*=0,\pi$. Let us denote Ω_N^* the reduced set of different values $\varphi_j^*\in]0,\pi[$. For fixed N, this set consists of the angles

$$\{\varphi_j^*\}=\left\{\frac{\pi}{2},\frac{\pi}{3},\ldots,\frac{\pi}{N-1}\right\} \tag{59}$$

and all multiples of these such that $0<\varphi_j^* d<\pi$. For instance, for $N=6$ we explicitly have

$$\Omega_6^*=\left\{\frac{\pi}{2},\frac{\pi}{3},\frac{\pi}{4},\frac{\pi}{5},\frac{2\pi}{3},\frac{2\pi}{5},\frac{3\pi}{4},\frac{3\pi}{5},\frac{4\pi}{5}\right\}. \tag{60}$$

In general,

$$\Omega_N^*=\left\{\varphi_j^*:\ \varphi_j^* k=\pi d,\ k=1,2,\ldots,N-1,\ d=1,2,\ldots,k-1\right\}, \tag{61}$$

with the condition that pairs d,k having the same ratio d/k are counted only once.

For fixed N, the total number of the points where $\Gamma_{\rm ch}$ diverges is given by

$$|\Omega_N^*| = \left(\sum_{k=2}^{N-1} \sum_{d(k)=1}^{k-1} 1 \right)', \tag{62}$$

where the prime means that different pairs d, k with the same ratio d/k are taken into account one time only in the sum. For $N = 3, 4, 5, 6, 7, 8, 9, 10, 100, 300$ we find, respectively, $|\Omega_N^*| = 1, 3, 5, 9, 11, 17, 21, 27, 3003, 27\,317$, where the last two examples have been computed numerically. Finding a recursive relation for $|\Omega_N^*|$ is not easy. Note that if $N_1 \equiv N_{\rm pr}$ is a prime number, then $\Omega^*_{N_{\rm pr}+1}$ will contain $N_{\rm pr} - 1$ new elements with respect to $\Omega^*_{N_{\rm pr}}$, viz.

$$\Omega^*_{N_1+1} \setminus \Omega^*_{N_1} = \left\{ \frac{\pi}{N_1}, \frac{2\pi}{N_1}, \ldots, \frac{(N_1-1)\pi}{N_1} \right\}, \tag{63}$$

so that $|\Omega^*_{N_{\rm pr}+1}| = |\Omega^*_{N_{\rm pr}}| + N_{\rm pr} - 1$. If N_1 is not a prime number, then $|\Omega^*_{N_1+1}| - |\Omega^*_{N_1}| < N_1 - 1$ since some elements of the set (63) are already present in $\Omega^*_{N_1}$. Therefore, to find an exact asymptotic behaviour of $|\Omega_N^*|$, one needs at least to know the distribution of the prime numbers on an interval $[1, N]$, which is a famous unresolved mathematical problem [19]. By using Mathematica, we find that for $N \leqslant 2000$, the cardinality of Ω_N^* grows quadratically with the system size N: specifically, $|\Omega_N^*| \approx 0.303\,86 N^2$.

4.2. NESS at $\Gamma_{\rm ch}$ singularities

On varying the twisting angle φ (the anisotropy being fixed at the value $\Delta = \cos\varphi$), the NESS everywhere converges, in the Zeno limit, to the pure SHS (6), except for φ given by the singular points (58), where the limiting NESS is mixed. This is well illustrated by figure 7, where the von Neumann entropy $S_{\rm VNE}(\varphi)$ tends to vanish everywhere except at the nine values of φ given by equation (60). For small polar angles θ, the convergence of the NESS to the SHS is faster—see figure 8—but the divergences of $\Gamma_{\rm ch}$, where the convergence fails, arise at the same points. For the particular value $\varphi_j^* = \pi/2$, and $\theta = \pi/2$, the NESS can be shown to be a completely mixed state of the form

$$\lim_{\Gamma\to\infty} \rho_{\rm NESS} = \frac{1}{2^{N-2}} \rho_L \otimes I_{2,3,\ldots,N-1} \otimes \rho_R, \qquad \text{for } \varphi = \pi/2, \tag{64}$$

where ρ_L, ρ_R are the reservoir polarizations—see section 4.1 of [20] for details. For other φ_j^*, the NESS converges to some unknown mixed states.

4.3. Source of $\Gamma_{\rm ch}$ singularities

All points of divergence of $\Gamma_{\rm ch}$ must be either due to divergence of K^{-1}, entering equation (51) directly, or the divergence of Λ entering the expression (51) through the terms $Q_{\alpha,k} = \langle\alpha|\,[\Lambda h^{01}, h^{k0}]\,|0\rangle$, or both [1]. Using Mathematica, we checked that each of the points (58) correspond to a divergence of either K^{-1} or the $Q_{\alpha,k}(\Lambda)$ terms. The partition of the singularities of $\Gamma_{\rm ch}$ between K^{-1} and Λ depends quite crucially on the value of the polar angle θ.

For $\theta \neq \pi/2$, we have $\det K \neq 0$ for any φ and any N; therefore, K^{-1} always exists, and all the points of divergence of $\Gamma_{\rm ch}$ are due to divergency of the terms $Q_{\alpha,k}(\Lambda)$.

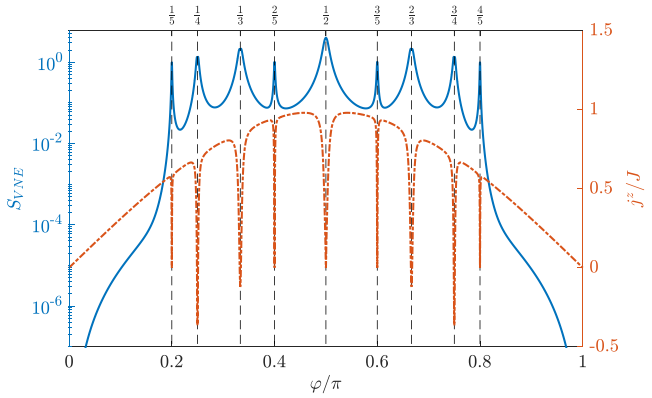

Figure 7. Von Neumann entropy of the NESS (solid blue line, left vertical scale) and steady-state magnetization current (dot-dashed red line, right vertical scale) as a function of the twisting angle φ. System parameters: $N = 6$, $\Delta = \cos\varphi$, $\theta = \pi/2$, $\Gamma = 500$. There are nine singular points characterized by peaks of $S_{\rm VNE}$ and nadirs of j^z, where the convergence of the NESS to a pure spin-helix state fails. These points coincide with those predicted theoretically—see equation (60). Note the symmetry around $\varphi = \pi/2$.

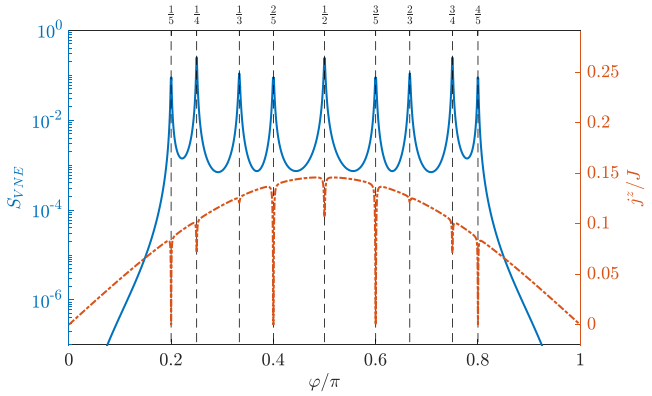

Figure 8. As in figure 7 but for $\theta = \pi/8$.

For $\theta = \pi/2$, K^{-1} is singular at the isolated points $\varphi_j^{**} \in \Omega_N^{(K)} \subset \Omega_N^*$, where

$$\Omega_N^{(K)} = \left\{ \varphi_j^{**} : \ \varphi_j^{**} 2k = \pi d, \ k = 1, 2, \ldots, \left\lfloor \frac{N-1}{2} \right\rfloor, \ d = 1, 2, \ldots, 2k-1 \right\}. \tag{65}$$

In this set, as in Ω_N^*, pairs d, k with the same ratio $d/(2k)$ are counted only once. The terms $Q_{\alpha,k}(\Lambda)$ diverge at the points of the complementary subset

$$\Omega_N^{(\Lambda)} = \Omega_N^* \setminus \Omega_N^{(K)}. \tag{66}$$

For example, in the case $N = 6$ we have

$$\Omega_6^{(K)} = \left\{ \frac{\pi}{2}, \frac{\pi}{4}, \frac{3\pi}{4} \right\}, \tag{67}$$

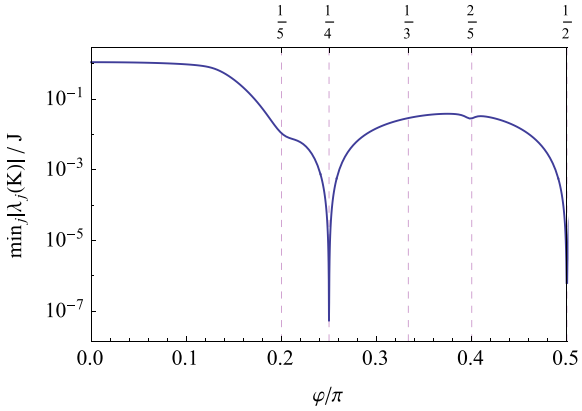

Figure 9. Minimum modulus of the eigenvalues of the matrix K as a function of the twisting angle φ for $N = 6$. The plot is symmetric with respect to $\varphi = \pi/2$ and $\varphi = 0$. Parameters: $\theta = \pi/2$, $\Delta = \cos\varphi$.

$$\Omega_6^{(\Lambda)} = \left\{ \frac{\pi}{3}, \frac{\pi}{5}, \frac{2\pi}{3}, \frac{2\pi}{5}, \frac{3\pi}{5}, \frac{4\pi}{5} \right\}. \tag{68}$$

In figure 9 we show the minimum modulus of the eigenvalues of the matrix K as a function of the twisting angle φ for $N = 6$ and $\theta = \pi/2$. Zeros are obtained exactly at the points of the set (67).

The number of points in $\Omega_N^{(\Lambda)}$ is smaller than the number of points where Λ, tout court, has a divergence—i.e. the points of degeneracy of h^{00}. This is easily understood if, instead of directly studying the divergence of the terms $Q_{\alpha,k}(\Lambda)$, we proceed as follows. Divergence of $\Gamma_{\rm ch}$ governed by the Λ matrix stems from an inconsistency of the linear system of equations for the coefficients $M_{\alpha 0}^{(1)}$ arising in the first order expansion of the NESS in powers of $1/\Gamma$ [1]. In the basis in which h^{00} is diagonal, this system has the form (see equation (A24) of [1])

$$(\lambda_\alpha - \lambda_0) M_{\alpha 0}^{(1)} = 2\mathrm{i}\kappa \langle \alpha | h^{01} | 0 \rangle , \qquad \alpha = 1, 2, \ldots, d_1 - 1. \tag{69}$$

Since $\kappa \neq 0$, the quantity $M_{\alpha 0}^{(1)}$ diverges if two conditions are simultaneously satisfied: (a) the eigenvalue λ_0 of h^{00} is degenerate, i.e. $\lambda_\alpha - \lambda_0 = 0$ for some $\alpha = 1, 2, \ldots, d_1 - 1$, and (b) for the corresponding α it results $\langle \alpha | h^{01} | 0 \rangle \neq 0$. Note that the sole degeneracy of λ_0 may not lead to a divergence of $\Gamma_{\rm ch}$.

Inspecting, for various finite N, the angles φ where both (a) and (b) conditions are satisfied, we recover the subset $\Omega^{(\Lambda)}$ given by equation (66). The case $N = 6$ with $\theta = \pi/2$ is shown in figure 10. Conditions (a) and (b) simultaneously hold at the points $\varphi/\pi = 1/5, 1/3, 2/5$ as well as in the symmetric points $\varphi/\pi = 3/5, 2/3, 4/5$ not shown in the plot.

We conclude that the NESS reached in the Zeno limit becomes pure for all φ, except at the singular points of the set (58), where two or more spins in the target spin-helix configuration become collinear. In figure 11 we plot $\Gamma_{\rm ch}(\varphi)$ evaluated according to equation (51). The characteristic dissipation shows divergence exactly at the points predicted by (58). Note that in the thermodynamic limit $N \to \infty$ the number of divergencies grows quadratically with the system size.

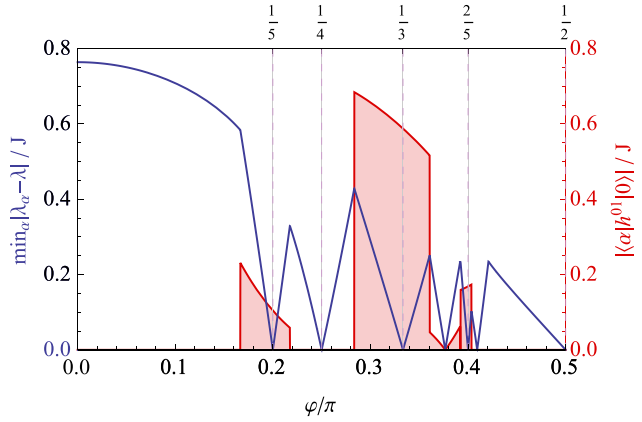

Figure 10. Gap of the h^{00} spectrum (solid blue line, left vertical scale) and corresponding matrix element $\langle\alpha|\,h^{01}\,|0\rangle$ (dashed red line with filling to the horizontal axis, right vertical scale) as a function of the twisting angle φ for $N = 6$. Note that the gap vanishes, and simultaneously $\langle\alpha|\,h^{01}\,|0\rangle \neq 0$ only at points $\varphi/\pi = 1/5, 1/3, 2/5$. The plot is symmetric with respect to $\varphi = \pi/2$ and $\varphi = 0$. Parameters: $\theta = \pi/2, \Delta = \cos\varphi$.

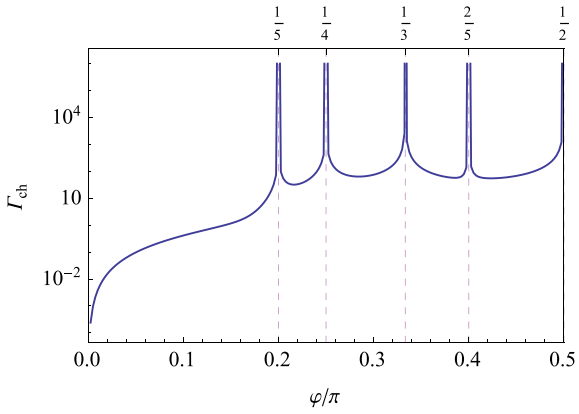

Figure 11. Characteristic dissipation $\Gamma_{\rm ch}$, computed according to equation (51), as a function of the twisting angle φ for $N = 6$. The plot is symmetric with respect to $\varphi = \pi/2$ and $\varphi = 0$. Parameters: $\theta = \pi/2, \Delta = \cos\varphi$.

5. Experimental scenarios

Finally, we comment on two hypothetical experimental scenarios. Using single atom techniques [21], it should be possible to realize systems with a fixed number N of spins $1/2$ coupled via Heisenberg exchange interaction, and to manipulate either the total twisting angle Φ (scenario A), or the anisotropy Δ (scenario B). For both cases, we assume that the dissipative strength Γ can also be controlled. Note that quantum Zeno dynamics [22] is well within reach of contemporary experimental setups [23].

5.1. Scenario A. Fixed anisotropy $|\Delta| < 1$*, varying boundary twist* Φ

It is clear from the previous discussion that an interesting case occurs if the anisotropy Δ obeys $-1 < \Delta < 1$ and $\Delta \neq 0$. For a quantum chain, the regime $-1 < \Delta < 1$ is referred to as critical, or an easy-plane regime, while the condition $\Delta \neq 0$ rules out the so-called non-interacting free-fermion case. The latter case corresponds to $\varphi = \pi/2$ and does not converge to a pure NESS for any N, see equation (64). Measuring any one of the NESS properties (a)–(c) discussed in section 1, for different total boundary twisting angles Φ, we will find a resonance-like behaviour corresponding to the existence of a spin-helix pure NESS. This will happen at the value $\Phi = \Phi_0$ given by

$$\Phi_0 = (N-1)\arccos\Delta. \tag{70}$$

The value of the characteristic dissipation above which the above resonance will be measured can be computed analytically using equation (51). We have seen that the characteristic value $\Gamma_{\rm ch}$ becomes large in proximity of the singular points φ_j^*, where a divergence of $\Gamma_{\rm ch}$ takes place—see equation (58). The larger the size of the system, the smaller the distance between two consecutive singular points φ_j^*. Therefore, we expect $\Gamma_{\rm ch}(\Delta)$, with Δ corresponding to some generic irrational value of $\varphi = \arccos\Delta$, to increase with the system size N, and to diverge in the thermodynamic limit.

5.2. Scenario B. Fixed boundary twist Φ*, varying anisotropy* $|\Delta| < 1$

This scenario is more spectacular then the previous one. For every generic fixed twisting angle Φ, such that Φ/π is irrational, there will be $N-1$ resonance values of the anisotropy, corresponding to the formation of SHSs in the Zeno limit. These resonance values are given by $\Delta(m) = \cos((\Phi + 2\pi m)/(N-1))$, $m = 0, 1, \ldots, N-2$. The characteristic dissipation, above which the phenomenon can be measured, will depend on m and on the closeness of the respective $\varphi = \arccos\Delta(m)$ to the nearest singular points φ_j^* of equation (58). By increasing the size of the system we will have two competing effects. The number of resonances will grow linearly with the size N, but the majority of the SHSs will become more difficult to measure due to the overall growth of $\Gamma_{\rm ch}$. Note, however, that SHSs with the effective smallest winding numbers, namely, $m = 0$ and $m = N-2$, become more accessible as the system size grows. In fact, we have observed in [14] that, for these winding numbers, $\Gamma_{\rm ch}(\epsilon)$, the characteristic dissipation at a chosen purity ϵ of the NESS decreases with increasing N.

6. Conclusions

We have shown that a boundary-driven Heisenberg spin chain in the critical regime $|\Delta| < 1$ exhibits, for large dissipation strength, a set of structural transitions in its non-equilibrium steady state between states with spatially smooth magnetization profile and spin-helix structures, where the local magnetization significantly changes from one site to another. Each spin-helix structure can be understood as a single generalized discrete Fourier harmonic, compatible with the boundary conditions imposed by the dissipation. Varying the anisotropy inside the critical easy-plane phase, $-1 < \Delta < 1$, and keeping sufficiently large dissipation strength, i.e. suppressing the boundary fluctuations, a complete set of these generalized discrete Fourier harmonics can be generated, one by one.

Note that with the help of SHSs (6) one can prepare a single spin in an arbitrary pure state, regardless of the length of the chain and the position of the spin, for any value of the

anisotropy. This requires manipulating boundary dissipation at the ends of the chain. For isotropic spin exchange an arbitrary single spin state at a distance can be generated with just one boundary dissipator [24]. From the quantum transport point of view, existence of SHSs makes it possible to reach ballistic current in a situation where typical current is diffusive or subdiffusive.

Interestingly, a structural transition to an SHS fails whenever two or more spins in the helix become collinear. Such a situation arises when the twisting angle governing the helix is a rational multiple of π and the spin chain is sufficiently long. At a deeper level, these breakups of convergence of the NESS to a pure state are related to divergence of the characteristic dissipation—a threshold value of the dissipation, above which the structural transitions can be observed. We have provided an explicit formula for the characteristic dissipation, and a detailed classification of its points of divergence.

The method we propose can be straightforwardly generalized, and can be tested on other systems, e.g. on spin chains with higher spins—see [18]. It would be interesting to see if spin-helix-like structures can be realized in $1D$ arrays of magnetic atoms [21].

Acknowledgments

Support from DFG grant is gratefully acknowledged. VP thanks the IBS Center of Theoretical Physics of Complex systems in Daejeon, Korea, where a part of this work was done, for hospitality.

Appendix. Dependence of $\Gamma_{\rm ch}$ on the polar angle θ. Solvable case $N = 3$

It is instructive to consider the simplest nontrivial chain with $N = 3$ spins. In this case, the Hilbert spaces $\mathcal{H}_0$ and $\mathcal{H}_1$ have dimensions $d_0 = 2^2$ and $d_1 = 2^1$ respectively. The matrix K is, therefore, a scalar, and—using equations (36), (52), (33), and (51)—we find

$$K = -2\left(2\cos(2\varphi)\sin^2(\theta) + \cos(2\theta) + 3\right). \tag{A.1}$$

Note that $K \leqslant 0$ for all $\theta,\ \varphi$ and $K = 0$ only for $\theta = \pi/2,\ \varphi = \pi/2$. For $\Gamma_{\rm ch}$ we obtain the remarkably simple expression

$$\Gamma_{\rm ch}^2 = 8\sin^4(\theta)\sin^2(\varphi)\tan^2(\varphi). \tag{A.2}$$

We conclude that for $N = 3$ the dependence of $\Gamma_{\rm ch}$ on θ is described by a multiplicative factor $\sin^2(\theta)$, which reaches its maximum at $\theta = \pi/2$.

For $N > 3$, the θ-dependence of $\Gamma_{\rm ch}$ is no longer multiplicative; however, it has the form

$$\frac{\Gamma_{\rm ch}(N,\varphi,\theta)}{\Gamma_{\rm ch}(N,\varphi,\pi/2)} = C_N(\varphi,\theta), \tag{A.3}$$

$$C_N(\varphi,\theta) = C_N(\varphi,\pi-\theta), \tag{A.4}$$

$$C_N(\varphi,\theta) \leqslant 1. \tag{A.5}$$

We have seen that $C_3(\varphi,\theta) = \sin^2(\theta)$, independent of φ. For $N > 3$, the function $C_N(\varphi,\theta)$ at fixed φ is always a symmetric function, $C_N(\varphi,\theta) = C_N(\varphi,\pi-\theta)$, which has an extremum at $\theta = \pi/2$. For most values of φ, $C_N(\varphi,\theta)$ has, as a function of θ, an absolute maximum at

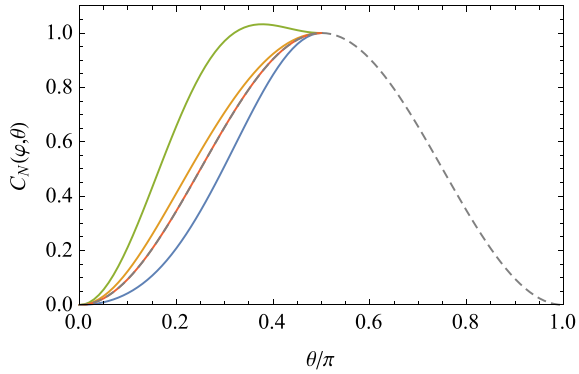

Figure A1. Function $C_N(\varphi,\theta)$ versus θ for $N=5$ and $\varphi=\pi/2+0.01, 2\pi/7, \pi/5, \pi/100$ (solid curves from bottom to top). The dashed gray line, shown for comparison, is $C_3(\varphi,\theta)=\sin^2\theta$.

$\theta=\pi/2$—see figure A1. For small $\theta\ll 1$, $C_N(\varphi,\theta)$ decreases as θ^2, making the respective dissipative pure state (6) easier to reach (given purity attained at smaller dissipative strengths). This is in accordance with physical intuition, since for small θ the SHS (6) corresponds to small deviations of the local magnetization vector from the $(0,0,1)$ direction, which are easier to sustain.

ORCID iDs

Carlo Presilla https://orcid.org/0000-0001-6624-4495

References

[1] Popkov V, Presilla C and Schmidt J 2017 *Phys. Rev.* A **95** 052131
[2] Gaudin M 2014 *The Bethe Wavefunction* (Cambridge: Cambridge University Press)
[3] Korepin V V E, Izergin A G and Bogoliubov N M 1993 *Quantum Inverse Scattering Method, Correlation Functions and Algebraic Bethe Ansatz* (Cambridge: Cambridge University Press)
[4] Žnidarič M 2011 *J. Stat. Mech.* P12008
[5] Žnidarič M 2011 *Phys. Rev. Lett.* **106** 220601
[6] Prosen T 2011 *Phys. Rev. Lett.* **107** 137201
[7] Prosen T 2015 *J. Phys. A: Math. Theor.* **48** 373001
[8] Breuer H P and Petruccione F 2002 *The Theory of Open Quantum Systems* (Oxford: Oxford University Press)
[9] Plenio M B and Knight P L 1998 *Rev. Mod. Phys.* **70** 101–44
[10] Clark S R, Prior J, Hartmann M J, Jaksch D and Plenio M B 2010 *New J. Phys.* **12** 025005
[11] Landi G T, Novais E, de Oliveira M J and Karevski D 2014 *Phys. Rev.* E **90** 042142
[12] Karevski D, Popkov V and Schütz G M 2013 *Phys. Rev. Lett.* **110** 047201
[13] Popkov V, Karevski D and Schütz G M 2013 *Phys. Rev.* E **88** 062118
[14] Popkov V and Presilla C 2016 *Phys. Rev.* A **93** 022111
[15] Bernevig B A, Orenstein J and Zhang S C 2006 *Phys. Rev. Lett.* **97** 236601
[16] Koralek J D, Weber C P, Orenstein J, Bernevig B A, Zhang S C, Mack S and Awschalom D D 2009 *Nature* **458** 610–3

[17] Winkler R 2003 *Spin–orbit Coupling Effects in Two-Dimensional Electron and Hole Systems* (*Springer Tracts in Modern Physics*) (Berlin: Springer)
[18] Popkov V and Schütz G M 2017 *Phys. Rev.* E **95** 042128
[19] Ingham A E 1990 *The Distribution of Prime Numbers* (*Cambridge Mathematical Library*) (Cambridge: Cambridge University Press)
[20] Popkov V 2012 *J. Stat. Mech.* P12015
[21] Toskovic R, van den Berg R, Spinelli A, Eliens I S, van den Toorn B, Bryant B, Caux J S and Otte A F 2016 *Nat. Phys.* **12** 656–60 (letter)
[22] Facchi P and Pascazio S 2008 *J. Phys. A: Math. Theor.* **41** 493001
[23] Schäfer F, Herrera I, Cherukattil S, Lovecchio C, Cataliotti F S, Caruso F and Smerzi A 2014 *Nat. Commun.* **5** 3194
[24] Žnidarič M 2016 *Phys. Rev. Lett.* **116** 030403